SAND2006-6347C
Proceedings of IMECE2006:
2006 ASME International Mechanical Engineering Congress and Exposition
Chicago, Illinois, November 5-10, 2006

IMECE2006-15169

VAN DER WAALS AND CAPILLARY ADHESION OF MICROELECTROMECHANICAL SYSTEMS

Frank W. DelRio[1,2], Maarten P. de Boer[2], Leslie M. Phinney[3], Chris J. Bourdon[3], and Martin L. Dunn[1]

[1]Department of Mechanical Engineering,
University of Colorado at Boulder, Boulder, Colorado 80309

[2]MEMS Devices and Reliability Physics Department,
[3]Microscale Science and Technology Department,
Sandia National Laboratories, Albuquerque, New Mexico 87185

ABSTRACT

Interfacial adhesion is an important factor in determining the performance and reliability of microelectromechanical systems (MEMS). Van der Waals dispersion forces are the dominant adhesion mechanism in the low relative humidity (RH) regime. At small roughness values, adhesion is mainly due to van der Waals dispersion forces acting across extensive non-contacting areas and is related to $1/D_{ave}^2$, where D_{ave} is the average surface separation. These contributions must be considered due to the close proximity of the surfaces, which is a result of the planar deposition technology. At large roughness values, van der Waals forces at contacting asperities become the dominating contributor to the adhesion. Capillary condensation of water has a significant effect on rough surface adhesion in the moderate to high RH regime. Above a threshold RH, which is a function of the surface roughness, the adhesion jumps due to meniscus formation at the interface and increases rapidly towards the upper limit of $\Gamma=2\gamma\cos\theta=144$ mJ/m^2, where γ is the liquid surface energy and θ is the contact angle.

INTRODUCTION

Silicon gained acceptance as a structural material after Petersen's review paper in 1982, which outlined the mechanical properties for single-crystal silicon and also provided a number of example structures to illustrate the potential for MEMS [1]. At the same time, researchers were investigating polycrystalline silicon (polysilicon) as a mechanical material and fabricated structures using a silicon dioxide sacrificial layer [2]. This surface-micromachining technique has been used over the years to form micron-scale complex mechanisms such as pressure transducers [3], micromotors for optical scanners [4], pin joints and springs [5], comb drive actuators [6], linear vibrometers [7], and hinges [8]. Because of the large surface-to-volume ratio in this regime, however, surface forces can dominate over inertial forces and cause mechanisms to adhere rather than perform their intended function. This unwanted adhesion, commonly called "stiction", occurs when the restoring forces of the compliant microstructures are unable to overcome interfacial forces such as capillary and van der Waals attractions. The primary objective of this work is to address the failure mechanisms associated with contacting surfaces, specifically adhesion due to van der Waals and capillary forces. By understanding the effects of surface topography (i.e., surface roughness) and environmental conditions (i.e., relative humidity) on the adhesion of micromachined surfaces, it should be possible to develop reliable, cost-effective MEMS for industrial applications.

SURFACE FORCES ON SIMPLE GEOMETRIES

To start, we review the effect of various surface forces on a few simple geometries, namely two flat surfaces and a sphere on a flat surface, both separated by a distance d. Capillary forces can develop between hydrophilic surfaces as a result of the relative humidity in the environment. The Kelvin radius r_k (i.e., the radius of curvature of a liquid meniscus in equilibrium with a vapor) is related to the RH by

$$r_k = \frac{\gamma v}{RT \ln(RH)} \quad (1)$$

where γ is the liquid-vapor surface energy, v is the molar volume, R is the gas constant, and T is the temperature ($\gamma v/RT$ = 0.53 nm for water at 300 K). For example, the Kelvin radius is -0.76 nm at 50% RH. The values are negative, indicating that the Laplace pressure

$$\Delta P = \frac{\gamma}{r_k} \quad (2)$$

across the liquid meniscus is negative and the capillary forces act to pull the surfaces together. The adhesion energy, or the work required to separate the surfaces, depends on the amount of evaporation or condensation during the separation process. de Boer and de Boer provide a review of the two extremes for the following geometries: two flat surfaces and a sphere on a flat surface [9]. In the first case, the volume of the liquid remains constant (i.e., no evaporation or condensation). This corresponds to a rapid separation of the interface, which prevents the capillary menisci from reaching thermodynamic equilibrium. For the constant volume case, the capillary force F_{cap} between two flat plates is related to the separation d by

$$F_{cap} = \frac{2\gamma d_o \cos\theta}{d^2} \pi x_d^2, \quad (3)$$

where d_o is the initial separation, θ is the contact angle between the meniscus and the surface, and x_d is the radius of the flat surface. Additionally, the capillary force F_{cap} between a sphere and a flat surface is given by

$$F_{cap} = 4\pi R\gamma \cos\theta \left(1 - \frac{d}{\sqrt{4r_k^2 \cos^2\theta + d^2}}\right), \quad (4)$$

where R is the radius of the sphere.

In the second case, the Kelvin radius r_k (and thus the Laplace pressure ΔP) of the liquid remains constant. This corresponds to a slow separation of the interface. As a result, the liquid at the interface is allowed to reach thermodynamic equilibrium via evaporation or condensation. For the constant Kelvin radius case, the capillary force F_{cap} between two flat plates is related to the separation d by

$$F_{cap} = \frac{\gamma}{r_k} \pi x_d^2, \quad (5)$$

while the capillary force F_{cap} between a sphere and a flat surface is given by

$$F_{cap} = 4\pi R\gamma \cos\theta \left(1 - \frac{d}{2|r_k|\cos\theta}\right). \quad (6)$$

Unlike capillary forces, van der Waals dispersion forces cannot be eliminated and pose a fundamental limit to the adhesion between micromachined surfaces. London showed that normal van der Waals forces can arise from a temporary dipole moment produced by the instantaneous positions of electrons in a molecule [10]. This temporary dipole polarizes the electron distribution of a nearby molecule, creating an attractive dispersion energy proportional to $1/r^6$, where r is the distance between the molecules. This theory, however, assumes the nearby molecule responds immediately to the temporary dipole and therefore only applies for separations less than 10 nm [11]. In reality, information regarding the electron distribution travels at the speed of light with wavelengths corresponding to the emission spectrum of the molecule [12]. Casimir and Polder demonstrated that the interaction energy between molecules becomes proportional to $1/r^7$ for distances larger than these wavelengths [13]. As a result, the Casimir force or retarded van der Waals force [14] governs at separations greater than 50 nm [11]. Assuming the forces are additive, the normal and retarded van der Waals forces between two smooth flat surfaces are

$$F_{vdW} = \frac{A}{6\pi d^3} \pi x_d^2 \quad (7)$$

and

$$F_{rvdW} = \frac{B}{d^4} \pi x_d^2, \quad (8)$$

respectively, where A is the Hamaker constant and B is the retarded van der Waals constant [12]. The normal and retarded van der Waals forces between a sphere and a flat surface are given by

$$F_{vdW} = \frac{AR}{6d^2} \quad (9)$$

and

$$F_{rvdW} = \frac{2\pi BR}{3d^3}, \quad (10)$$

respectively [12]. A gradual transition from normal to retarded van der Waals forces occurs between these separations [11,15] according to the following function

$$g = 1 - \frac{2d}{c} + \frac{6d^2}{c^2} + \frac{12d^3}{c^3} - \frac{12d^3(d+c)}{c^4} \ln\left(1 + \frac{c}{d}\right), \quad (11)$$

where $c = b\lambda/2\pi$ is a constant based on a characteristic wavelength λ=100 nm and an additional constant b=3.1 [15].

The capillary and van der Waals forces acting across an area of πx_d^2=1 μm^2 are plotted as a function of surface separation in Fig. 1. For capillary forces (constant volume case), we assume a contact angle of θ=0°, surface energy of γ=72 mJ/m^2 for water, relative humidity of 50%, and an initial separation of $d_o = 2r_k\cos\theta$. For van der Waals forces, we use d_{co}=0.2 nm as the initial separation [16] and A=5×10^{-20} J as the Hamaker constant.

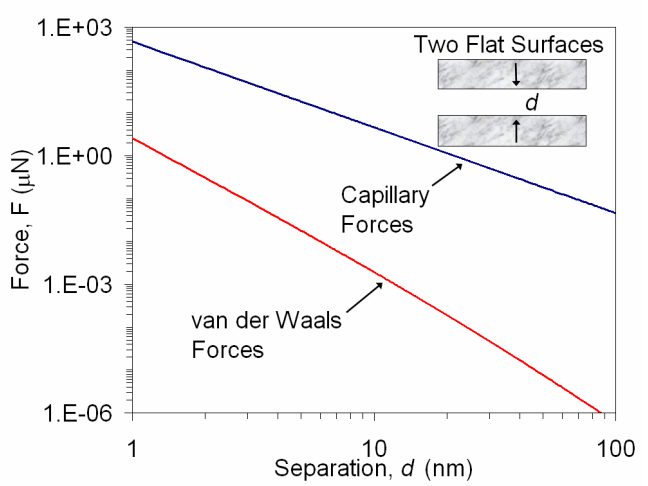

Figure 1: Capillary and van der Waals forces between two flat surfaces with a 1 μm^2 area separated by a distance d. Even at relatively low RH values (50% RH), capillary forces are shown to dominate van der Waals forces by several orders of magnitude.

In comparison, the restoring force for spring-suspended MEMS devices deflected by 1 μm in the transverse direction is between 10^{-3} and 10 μN [17]. Based on these results, the following conclusions can be made regarding the adhesive and restoring forces on the micron-scale. Even at relatively low RH values (50% RH), capillary forces are shown to dominate van der Waals forces by several orders of magnitude. Van der Waals forces, however, are still sufficient to overcome restoring forces at small surface separations. Therefore, it becomes necessary to understand and manipulate these forces to avoid adhesion-induced failures in MEMS devices.

While the flat plate constitutive laws provide insight into the magnitude of the attractive forces as a function of surface separation, they neglect the actual surface topography. Interfacial forces are reduced several orders of magnitude as a result of surface roughness, which reduces the interfacial area to the contacting asperities. Standard rough surface adhesion models account for surface roughness by assuming a statistical distribution of summit heights in contact with a rigid flat plane [18,19]. These models account for surface forces at or around the contact areas, which is a valid assumption for micron-scale spheres or surface roughness. As a result of the planar deposition technology in MEMS, however, surfaces normally exhibit nanometer-scale roughness. Thus, all points along the interface are separated by less than 100 nm and the adhesion contribution from these non-contacting areas can no longer be neglected. The size and separation of these surfaces is further reduced in nanoelectromechanical systems (NEMS). In this regime, the surface forces across non-contacting areas will require even more attention to prevent adhesion-induced failures. Therefore, it becomes necessary to develop new theoretical and experimental techniques that take into account adhesion contributions from both contacting and non-contacting areas.

EXPERIMENTAL TECHNIQUES

Several experimental techniques have been used to analyze the adhesion between surfaces (e.g., surface force apparatus, atomic force microscope, and single/double cantilever beam specimens). The surface force apparatus (SFA) is an instrument used to measure interfacial phenomena between two crossed mica cylinders in various environments [11,12]. Though mica is the primary surface for the measurements, it is also possible to deposit optically smooth metals or polymers [20]. The force sensitivity and distance resolution are about 10 nN and 0.1 nm, respectively. The atomic force microscope (AFM) can also measure interfacial forces via a sharp tip (radius of ~10-100 nm) attached to the end of a compliant cantilever [21]. The separation between the cantilever and sample is varied with 0.1 nm resolution, while the force is measured by considering the deflection of the cantilever beam. The resulting force-displacement curve can be integrated to find the work of adhesion in a variety of environments, including liquids [22] and ultrahigh vacuum [23]. While more of a test structure than an instrument, the double cantilever beam has long been used to measure adhesion; a stable cleavage crack is introduced through a sample (force or displacement controlled) and the new interfacial area is measured [24-26]. A related device can be fabricated using standard micromachining techniques as shown in Fig. 2. The cantilever beam test method has an important advantage over the other techniques: it uses the actual mating micromachined surfaces to measure the adhesion, as opposed to only one surface and a cylinder/tip. For this reason, the cantilever technique will be used throughout this work.

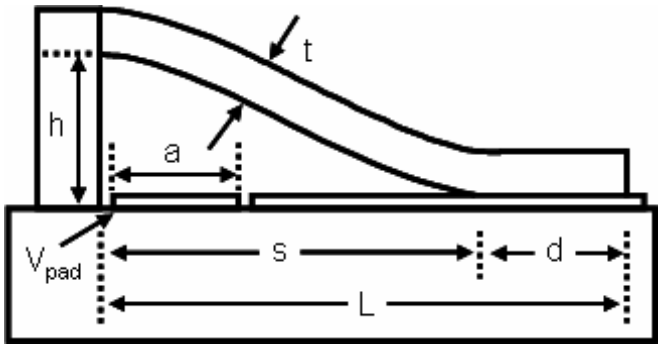

Figure 2: A schematic representation of an s-shaped cantilever beam.

The microcantilevers were fabricated by standard surface micromachining techniques [27]. Nanotexturing of the lower layer of polysilicon, which defines the landing pad, was accomplished by thermal oxidation in dry O_2 at 900°C for increasing times. The main texturing effect is due to grains that protrude upwards from the surface. This occurs because the polysilicon grains are randomly oriented and dry oxidation in

the linear regime proceeds at different rates on the various orientations of silicon.

The microcantilevers are supported by a step-up support post and are electrically connected to the landing pad. An actuation pad is also defined in the landing pad level. After fabrication, the structures were released in hydrofluoric acid, which removes the sacrificial and thermal oxide layers. To render the cantilevers freestanding, we applied a hydrophobic monolayer coating of perfluorodecyltrichlorosilane (FDTS, $F(CF_2)_8(CH_2)_2SiCl_3$) to analyze van der Waals adhesion [28] and used a laser irradiation process to consider capillary adhesion [29]. Critical cantilever dimensions, as indicated in Fig. 2, include gap height *g*, thickness *t*, width *w*, length *L* and actuation pad length *a*. Using the terminology of linear elastic fracture mechanics, we refer to the open, unattached section of the beam as the crack length *s*. The gap g=1.90 μm and thickness t=2.62 μm were determined from freestanding cantilevers using profilometry. Mask dimensions were w=30 μm, a=81.5 μm and L =1500 μm.

VAN DER WAALS ADHESION

To examine van der Waals adhesion, we brought freestanding cantilevers into contact with the substrate by modulating the voltage on the actuation pad. Using phase-stepping interferometry, the full deflection curve of the cantilevers was determined to nanometer-scale accuracy. The resulting interferograms are shown in Fig. 3 for cantilevers with an applied load of V_{pad}=50 V. They qualitatively indicate a decrease in adhesion for an increase in surface roughness.

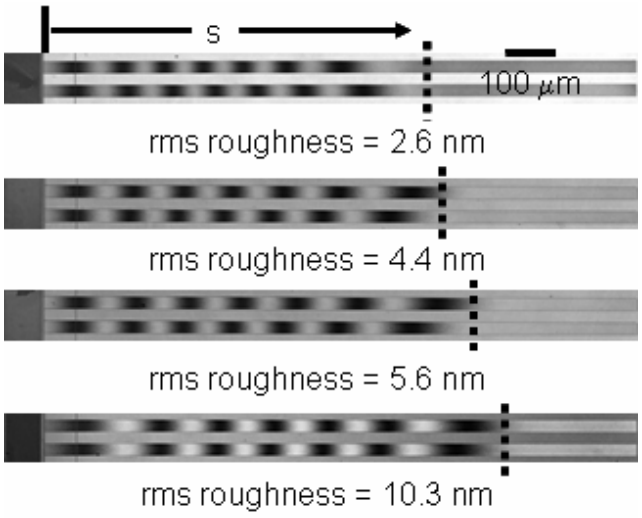

Figure 3: Interferograms of cantilever beams at an actuation voltage of V_{pad}=50 V, which qualitatively indicate a decrease in interfacial adhesion for an increase in surface roughness.

The adhesion energy can be extracted from beams under electrostatic loading by comparing experimental deflections to finite element method (FEM) simulations [30,31]. The FEM simulations include the electrostatic loading (with fringing field correction), the beam mechanical properties and the support post compliance. With these parameters known, adhesion is the only free parameter and is determined by a best fit to the measured deflection data. Typical best fit rms errors were 5 nm/pixel. Adhesion results for the different surface roughnesses are shown in Fig. 4. The adhesion data is plotted versus D_{ave}, the average surface separation. For each value of D_{ave}, Γ values were determined from two different cantilevers at applied voltages of V_{pad}=0 to 60 V.

Experimentally, the adhesion decreases from 8.0 to 2.1 μJ/m^2 as the roughness increases from 2.6 to 10.3 nm rms, as seen in Fig. 4. This decrease is not as large as predicted by [32] $\Gamma=A/12\pi D_{rms}^2$ (i.e., only a factor of 4 instead of 16). Testing was conducted in air at a relative humidity of ~30%. We have observed no effect of RH on testing results up to 80% RH for these coatings [30]. Scanning probe studies between a hydrophilic and hydrophobic surface have also shown no dependence of adhesion pull-off force on RH [33,34]. Therefore, capillary condensation, which dominates adhesion of hydrophilic surfaces [35], does not play a role in these experiments. The top and bottom surfaces are electrically grounded and consist of degenerately-doped polysilicon with a negligible contact potential difference. Consequently, electrostatic forces in the contact zone *d* are insignificant. Thus, the adhesion is primarily due to van der Waals dispersion forces. Complete details regarding these measurements and results are given elsewhere [36].

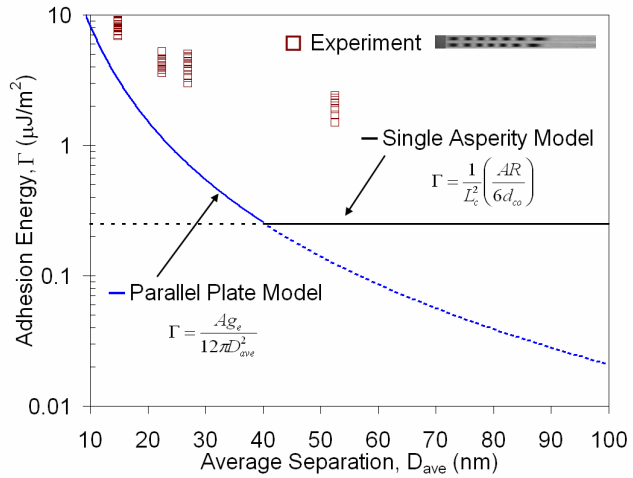

Figure 4: Adhesion results for the different surface roughnesses. Experimentally, the adhesion decreases from 8.0 to 2.1 μJ/m^2 as the roughness increases from 2.6 to 10.3 nm rms.

CAPILLARY ADHESION

To measure capillary adhesion, we brought the cantilevers into contact with the substrate at 0% RH with an actuation voltage of V_{pad}=100 V. The applied load was subsequently removed, which resulted in beams adhered to the substrate in the s-shaped position. The RH within the chamber was then

increased from 0% to 95% RH in 5% RH increments. The resulting interferograms of cantilever beams with a landing pad roughness of 2.6 nm rms are shown in Fig. 5. The crack length was approximately *s*=950 μm at low RH, which can be attributed to van der Waals dispersion forces acting across extensive non-contacting areas of the interface [36]. The crack length subsequently decreased to *s*=350 μm at 70% RH, *s*=200 μm at 85% RH, *s*=140 μm at 90% RH, and *s*=110 μm at 95% RH due to capillary condensation.

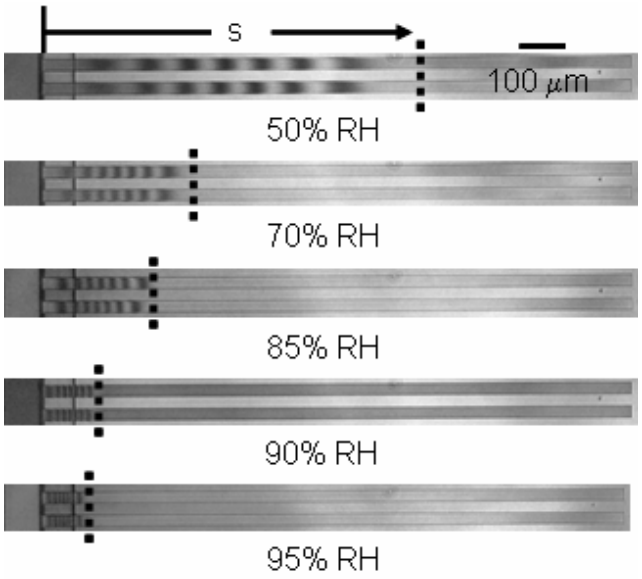

Figure 5: Interferograms of cantilever beams with a landing pad roughness of 2.6 nm rms as a function of RH. The crack length was approximately s=950 μm at low RH, which can be attributed to van der Waals dispersion forces acting across extensive non-contacting areas of the interface The crack length decreased to s=350 μm at 70% RH, s=200 μm at 85% RH, s=140 μm at 90% RH, and s=110 μm at 95% RH due to capillary condensation.

The adhesion energy was extracted by comparing the experimental deflections to finite element method simulations [30,31]. Adhesion results for cantilevers with landing pad roughnesses ranging from 2.6 to 10.3 nm rms are shown in Fig. 6. As the landing pad roughness increases, the RH at which the adhesion initially jumps due to capillary condensation also increases. Once the initial jump occurs, the adhesion increases towards the upper limit of $\Gamma=2\gamma\cos\theta=144$ mJ/m^2. Future work includes analyzing the experimental data via a simple model based on the measured surface topography and the constitutive laws presented in the earlier section.

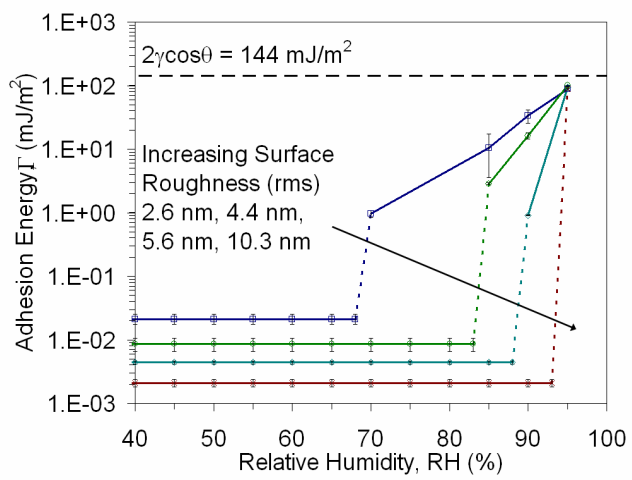

Figure 6: Adhesion energy as a function of RH for landing pad roughnesses ranging from 2.6 to 10.3 nm rms. The maximum adhesion energy due to capillary condensation $\Gamma=2\gamma\cos\theta=144$ mJ/m^2 is shown for reference.

CONCLUSIONS

Interfacial adhesion is an important factor in the performance and reliability of contacting MEMS. To explore this phenomenon between micromachined surfaces, we performed microcantilever experiments as a function of surface roughness and RH. At small roughness values, adhesion is mainly due to van der Waals dispersion forces acting across extensive non-contacting areas and is related to $1/D_{ave}^2$. At large roughness values, van der Waals forces at contacting asperities become the dominating contributor to the adhesion. In addition, topographic correlations between upper and lower surfaces, which are the result of the conformal nature of the sacrificial layer, must be considered to understand adhesion completely. In addition, the experimental data indicates a strong correlation between surface roughness and capillary condensation. As the landing pad roughness increases, the RH at which the adhesion initially jumps due to capillary condensation also increases. Once the initial jump occurs, the adhesion increases towards the upper limit of $\Gamma=2\gamma\cos\theta$. In addition to the aforementioned interfacial forces, it is also important to note that particulates can strongly influence interfacial adhesion between micromachined surfaces by changing their average separation [37].

ACKNOWLEDGMENTS

The authors would like to thank the Microelectronics Development Laboratory (MDL) staff at Sandia National Laboratories for fabricating the samples, Alex Corwin for help in collecting and interpreting experimental data, and W. R. Ashurst (Auburn University) for useful discussions and building the glass DC plasma generator. Sandia is a multiprogram laboratory operated by Sandia Corporation, a Lockheed Martin Company, for the United States Department of Energy's

National Nuclear Security Administration under contract DE AC04-94AL85000.

REFERENCES

1. K. E. Petersen, Proc. IEEE. **70(5)**, 420 (1982).
2. R. T. Howe and R. S. Muller, Proc. Electrochemical Society Spring Meeting, Montreal, Quebec. 184 (1982).
3. H. Guckel and D. W. Burns, IEEE Int. Electron Devices Meeting, San Francisco, CA. 223 (1984).
4. K. Deng, H. Miyajima, V. Dhuler, M. Mehregany, S. W. Smith, F. L. Merat, and S. Furukawa, Proc. 1994 Solid-State Sensor and Actuator Workshop, Hilton Head '94, 234 (1994).
5. L. S. Fan, Y. C. Tai, and R. S. Muller, IEEE Trans. Electron Devices **35**, 724 (1988).
6. W. C. Tang, T. C. H. Nguyen, M. W. Judy, and R. T. Howe, Sens. Actuators A Phys. **21-23**, 328 (1990).
7. A. P. Lee, D. J. Nikkel, and A. P. Pisano, Proc. 7th Int. Conf. Solid-State Sensors and Actuators, Transducers '93, Yokohama, Japan, 46 (1993).
8. K. S. J. Pister, M. W. Judy, S. R. Burgett, and R. S. Fearing, Sens. Actuators A Phys. **33**, 249 (1992).
9. M. P. de Boer and P. C. T. de Boer, *in preparation* (2006).
10. F. London, Trans. Faraday Soc. **33**, 8 (1937).
11. J. Israelachvili and D. Tabor, Proc. Roy. Soc. Lond. A **331**, 19 (1972).
12. D. Tabor and R. H. S. Winterton, Proc. Roy. Soc. Lond. A **312**, 435 (1969).
13. H. B. G. Casimir and D. Polder, Phys. Rev. **73(4)**, 360 (1948).
14. F. M. Serry, D. Walliser, and G. J. Maclay, J. Appl. Phys. **84(5)**, 2501 (1997).
15. A. Anandarajah and J. Chen, J. Colloid Interface Sci. **176**, 293 (1995).
16. J. Israelachvili, Intermolecular and Surface Forces (Academic Press, New York, NY, 1992).
17. R. Maboudian and R. T. Howe, J. Vac. Sci. Technol. B **15(1)**, 1 (1997).
18. K. N. G. Fuller and D. Tabor, Proc. Roy. Soc. Lond. A **345,** 327 (1975).
19. D. Maugis, J. Adh. Sc. Tech. **10(2)**, 161 (1996).
20. R. A. Quon, R. F. Knarr, and T. K. Vanderlick, J. Phys. Chem. **103**, 5320 (1999).
21. R. W. Carpick and J. D. Batteas, *Handbook of Nanotechnology*, edited by Bhushan, B. (Springer-Verlag, Berlin, 2004).
22. O. Marti, B. Drake, and P. K. Hansma, Appl. Phys. Lett. **51(7)**, 484 (1987).
23. L. Howald, E. Meyer, R. Lüthi, H. Haefke, R. Overney, H. Rudin, and H. -J. Güntherodt, Appl. Phys. Lett. **63(1)**, 117 (1993).
24. J. W. Obreimoff, Proc. Roy. Soc. London A **127**, 290 (1930).
25. A. I. Bailey, J. Appl. Phys. **32**, 1407 (1961).
26. D. H. Roach, S. Lathabai, and B. R. Lawn, J. Am. Ceram. Soc. **71(2),** 97 (1988).
27. J. J. Sniegowski and M. P. de Boer, Annual Rev. Mat. Sci. **30**, 299 (2000).
28. U. Srinivasan, M. R. Houston, R. T. Howe, and R. Maboudian, J. Microelectromech. Syst. **7(2)**, 252 (1998).
29. J. W. Rogers, T. J. Mackin, and L. M. Phinney, J. Microelectromech. Syst. **11(5)**, 512 (2002).
30. M. P. de Boer, J. A. Knapp, T. A. Michalske, U. Srinivasan, and R. Maboudian, Acta Mat. **48**, 4531 (2000).
31. J. A. Knapp and M. P. de Boer, J. Microelectromech. Syst. **11(6)**, 754 (2002).
32. M. R. Houston, R. T. Howe, and R. Maboudian, J. Appl. Phys. **81(8)**, 3474 (1997).
33. X. Xiao and Q. Linmao, Langmuir **16**, 8153 (2000).
34. M. He, A. S. Blum, D. E. Aston, C. Buenviaje, R. M. Overney, and R. Luginbuhl, J. Chem. Phys. **114(3)**, 1355 (2001).
35. M. P. de Boer, P. J. Clews, B. K. Smith, and T. A. Michalske, Mat. Res. Soc. Symp. Proc. **518**, 131 (1998).
36. F. W. DelRio, M. P. de Boer, J. A. Knapp, E. D. Reedy, P. J. Clews, and M. L. Dunn, Nature Materials **4**, 629 (2005).
37. F. W. DelRio, M. L. Dunn, B. L. Boyce, A. D. Corwin, and M. P. de Boer, J. Appl. Phys. **99**, 104304 (2006).